Rheological, Mechanical, Optical, and Transport Properties of Blown Films of Polyamide 6/Residual Monomer/ Montmorillonite Nanocomposites

Cesar A. G. Beatrice,[1] Marcia C. Branciforti,[1] Rosa M. V. Alves,[2] Rosario E. S. Bretas[1]

[1]*Universidade Federal de São Carlos, Departamento de Engenharia de Materiais—Rodovia Washington Luís, Km 235, C.P. 676, São Carlos, SP 13565-905, Brazil*
[2]*Instituto de Tecnologia de Alimentos, Centro de Pesquisa e Desenvolvimento de Embalagens—Avenida Brasil, 2880, C.P. 139, Campinas, SP 13070-178, Brazil*

Received 6 August 2009; accepted 29 November 2009
DOI 10.1002/app.31898
Published online 22 February 2010 in Wiley InterScience (www.interscience.wiley.com).

ABSTRACT: Exfoliated nanocomposites of polyamide 6 (PA6) with residual monomer and an organically treated montmorillonite (3 and 5 wt %) were produced by twin-screw extrusion. The composites had their steady state, dynamic, and transient rheological properties measured by parallel-plates rheometry; their exfoliation level was characterized by wide angle X-rays diffraction (WAXD) and transmission electron microscopy (TEM). The characterization showed as follows: (i) the nanoclay's lamellas were well dispersed and distributed thru the PA6, (ii) the postpolymerization of the residual monomer produced more branched chains than linear ones in the pure PA6, (iii) the nanoclay's lamellas acted as entanglement points in the nanocomposites, and (iv) the molecular weight of the PA6 in the nanocomposites decreased. Blown films of the nanocomposites were produced by single screw extrusion; the die pressure during the film blowing of the nanocomposites strongly decreased. The tensile mechanical properties of the blown films were also measured. Along the machine direction (MD), the best mechanical properties were obtained with the 5 wt % nanocomposite, whereas along the transverse direction (TD), the 3 wt % nanocomposite had the best behavior. The glass transition temperature (T_g) of the blown films was measured by dynamic mechanical thermal analyses (DMTA). The 5 wt % nanocomposite had the highest T_g of all the films. The optical properties were measured by spectrophotometry; the nanoclay decreased the films' haze, but the level of transmittance was not affected. The water vapor and oxygen permeability rates of the nanocomposites films were found to be lower than in the pure PA6 blown film as a result of a tortuosity effect. J Appl Polym Sci 116: 3581–3592, 2010

Key words: nanocomposites; blown films; polyamide 6; rheological properties; transport properties; mechanical properties

INTRODUCTION

The use of blown films has increased the efficiency of the food marketing and other products.[1] In this context, nanocomposites have a fundamental role, as these materials have better mechanical, thermal, and barrier properties than the pure polymer.[2] The nanocomposites are characterized by the use of a reinforcement agent with nanometric dimensions, which is added in very small quantities. When these materials are processed as blown films, besides the improvement on those properties, it is expected that the film has also good optical properties.

To produce a blown film, it is necessary that the material has a high ability to withstand the tensions developed during the blowing operation. The blown ability depends on high-melt strength or an equivalent rheological property, like elongational viscosity, zero shear viscosity, or storage modulus. As it is known, these rheological properties are dependent on molecular weight, molecular weight distribution, branches amount, nanofiller concentration, and its dispersion.[3] Thus, layered nanoclays, for example, which are composed of extremely thin, sheet-like platelets with very large surface areas and high aspect ratios, can alter the rheological properties of the polymer matrix.[4] Other rheological properties like the viscoelastic properties can also give information about the degree of nanoparticle's exfoliation in the polymeric matrix.[5]

The reinforcement of a polymer by layered nanoclay in blown films shows that exfoliated samples usually have an increase in tensile modulus without a significant reduction in tear strength and film extensibility; also, the gas permeability is reduced due to the biaxial orientation of the clay's platelets.[6] Therefore, the processing conditions during the blowing operation influence the mechanical properties. These processing conditions are dependent on

Correspondence to: R. E. S. Bretas (bretas@power.ufscar.br).
Contract grant sponsors: FAPESP.

the rheological properties of the material; thus, to optimize the film blowing process, correlations between rheological properties, microstructure and mechanical properties should be sought.[7] Literature, however, does not present many works on the study of these correlations.

Regarding polyamide 6 nanocomposites, for example, Baldi et al.[8] investigated the rheological behavior under shear and extension at high strain rates of a high-molecular weight polyamide 6/organo-montmorillonite nanocomposite, obtained by melt blending. In shear flow, the nanocomposite had a lower viscosity than the neat PA6, because of two cooperative effects: slip processes at the interface between the polymer melt and the aligned organo-clay particles and chemical degradation processes undergone by the PA6 chains. In elongation, the nanocomposites were more viscous, depending on the organo-clay content; this behavior was attributed to the impediment promoted by the organo-clay particles against the extensional deformation. The effectiveness of this impediment was also correlated to the alignment level of the organo-clay particles along the stretching direction.

The method to disperse the clay is also an important factor affecting the rheological and mechanical properties of PA6 nanocomposites. Tung et al.[9] investigated the rheological and mechanical properties of pure PA6 and its nanocomposites with an organically modified montmorillonite; the nanocomposites were produced by *in situ* polymerization and melt blending. A broad organoclay length distribution was observed in the composites prepared by melt blending, due to extensive damage promoted by the high shearing forces generated during screw rotation. During the rheological measurements, the melt-blended nanocomposite exhibited a more shear thinning behavior than the *in situ* nanocomposite, probably because in the first ones the interaction forces between the clay platelets and the polymer matrix were physical, whereas in the latter, they were formed by covalent bonds. These interactions promoted better clay dispersion in the *in situ* materials. Best dispersion led to a better modulus; however, the presence of agglomerates affected the failure properties. These agglomerates acted as stress concentrators, leading to an earlier initiation of the crack during tension.

Picard et al.[10,11] studied PA6/organo-montmorillonite membranes prepared by film blowing using clay contents between 0 and 18 wt %. The barrier properties to different penetrants were measured. Nanocomposites exhibited superior barrier properties to helium, dihydrogen, dioxygen, and water in comparison to the pure PA6 film. The permeability was found to be independent of the penetrant molecule showing that a tortuosity effect was at the origin of the improved barrier properties. All the silicate layers lied in the plane of the film, which corresponded to an optimal orientation for increased barrier properties. The crystalline morphology of the PA6 was shown to be slightly dependent of the nanocomposite composition. Consequently, the permeation properties were correlated to the clay content and dispersion.

Alexandre et al.[12] studied the mechanical and water barrier properties of polyamide 12/organo-montmorillonite membranes, obtained by compression molding. Depending on the clay amount and rotation speed during the composite preparation, two different structures were obtained: a partially intercalated structure and a partially exfoliated structure. In agreement with the tortuous path model, the water permeability and the diffusivity decreased with increasing clay content up to 2.5%, for both structures. However, beyond a clay content of 2.5% (for the partially intercalated nanocomposites) and until 4% (for the partially exfoliated nanocomposites) the permeability no longer decreased, but increased. This effect was higher for the partially intercalated structure than for the partially exfoliated structure. However, the best permeability values were obtained with the partially exfoliated nanocomposite.

In this work, blown films of PA6/residual monomer/montmorillonite nanocomposites, with 3 and 5 wt % of nanoclay, were produced to study the influence of the processing conditions on their rheological, mechanical, transport, and optical properties.

EXPERIMENTAL

Materials

An extrusion grade of polyamide 6, Technyl C 402*M* from Rhodia Engineering Plastics, was chosen as matrix of the nanocomposites. This resin had residual monomer (0.60 wt %), density of 1.14 g/cm^3, melting temperature of 222°C, melt flow index of 2.5 g/10 min (235°C/2.16 kg), a concentration of carboxyl terminal groups of 35 Meq/kg, and a concentration of amine terminal groups also of 35 Meq/kg.[13–15]

The nanoclay was an organically modified montmorillonite (MMT) Cloisite® 30B (C30B) from Southern Clay Products Inc with density of 0.36 g/cm^3. The original gallery's distance was 1.85 nm. The modification was done with a surfactant, a quaternary ammonium salt, which has unsaturated aliphatic chains with two hydroxyl groups, named diethanol-methyl-tallow quaternary ammonium salt. The chemical structure of the surfactant is shown in Figure 1;[16] the surfactant concentration was 900 Meq/kg.

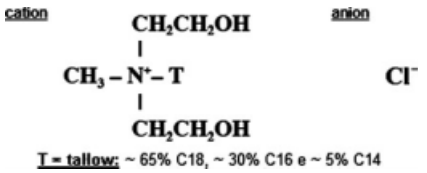

Figure 1 Chemical structure of the Cloisite® 30B surfactant.[16]

Thermal characterization

Thermogravimetric experiments to evaluate the organoclay's thermal degradation were done in a high resolution TA HiRes TGA 2950 analyzer using a heating rate of 20°C/min, from room temperature to 500°C, under N_2 atmosphere.

Preparation of the nanocomposites

The PA6/residual monomer pellets (sample **Pure PA6**) were pulverized using a cryogenic mill from Micron Powder Systems, model Mikro-Bantam. Both materials PA6/residual monomer and C30B were dried at 80°C for 14 h before melt blending. Nanocomposites with 3 and 5 wt % of nanoclay (samples **PA6 + 3% C30B** and **PA6 + 5% C30B**, respectively) were produced in a modulated twin screw extruder model ZSK30 from Werner and Pfleiderer, with 30 mm of diameter and 1065 mm of length thru a cylindrical die. A medium dispersive screw profile, designed with transport and kneading block elements and one turbine element at the end of the melting zone was used. A scheme of this profile is shown in Figure 2. The minimum ($\dot{\gamma}_{min}$) and maximum ($\dot{\gamma}_{max}$) shear rates due to drag flow were ~ 30 s^{-1} in the transport elements and ~ 1900 s^{-1} in the kneading blocks; they were calculated by the following equations:

$$\dot{\gamma}_{min} = \frac{\pi \cdot D \cdot N}{h_{max,transport}} \quad (1)$$

$$\dot{\gamma}_{max} = \frac{\pi \cdot D \cdot N}{h_{min,kneading}} \quad (2)$$

where D is the screw diameter, N is the screw rotation, $h_{max,transport}$ is the maximum flight height in the transport elements, and $h_{min,kneading}$ is the minimum available height for polymer flow in the kneading blocks.

The PA6/residual monomer and the C30B were fed together in the second feeder (at a PA6-residual monomer/C30B mass ratio of 90/10 and 94/6), whereas the remaining PA6/residual monomer (to obtain the 3 wt % and 5 wt % C30B concentration) was fed at the first feeder. The temperature range was set between 250 and 260°C and the screw velocity was set at 120 rpm; the mass flow rate was 4 kg/h, which resulted in a residence time of ~2 min.

To observe the effect of the thermomechanical history on the pure PA6/residual monomer during processing, the **Pure PA6** sample was also extruded at the same extrusion conditions than the nanocomposites, producing sample **Extruded PA6**.

Film blowing

Before film blowing, the **Pure PA6** sample and all extruded materials were dried at 80°C for 14 h. The film blowing was produced in a single screw extruder with a spiral die, model 25 × 30D from Miotto, with screw diameter of 25 mm and screw length of 750 mm. The spiral die had an external diameter of 80.0 mm, an internal diameter of 78.4 mm, and an extended length of 640 mm. The screw compression rate in half the length was 3.4. The temperature range was set between 240 and 250°C, the screw velocity was set at 65 rpm, and the velocity of the take up rollers, V_e, at 4 m/min. The mass rate Q (calculated by weighting the mass of the film extruded during 1 min) was 50 g/min. Thus, the velocity at the die exit, V_d, was calculated from eq. (3):

$$Q/\rho = V_d \cdot A_M \quad (3)$$

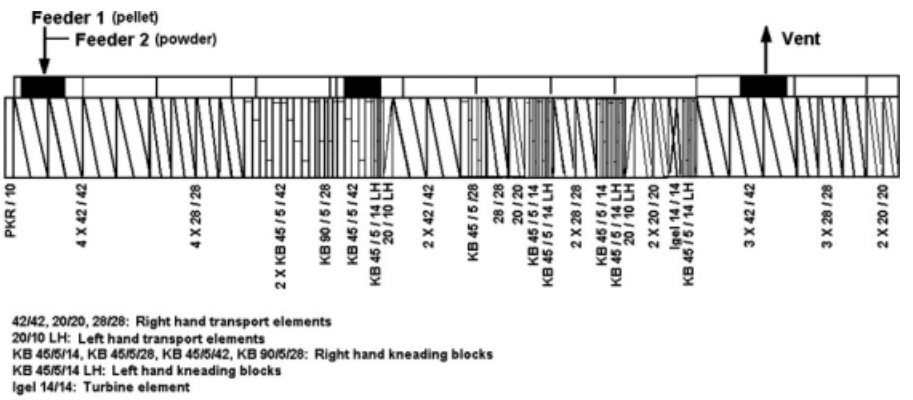

Figure 2 Profile of the twin screw extruder used in this work.[13]

in which ρ was the PA6 density and A_M the transversal area of the spiral die. V_d was found to be 0.22 m/min. Thus, the TUR ratio, defined as TUR = V_e/V_d, was found to be 18.0, whereas the BUR ratio, defined as BUR = R_f/R_d, where R_f and R_d are the film and die radius, respectively, was equal to 1.0.

The average thickness of the films was 50.0 μm (±5.7 μm) and the average diameter was 80.0 mm (±2.7 mm). The pressure developed at the extruder die during the film blowing operation was also monitored.

Characterization by wide angle X-ray diffraction (WAXD)

The extent of clay intercalation/exfoliation was determined by WAXD using a Siemens model D5000 diffractometer with CuKα radiation (λ = 1.5458 E) operating at 50 kV and 30 mA. Samples were scanned between 1 and 10° at a rate of 1°/min. Measurements were recorded at each 0.02°.

Morphological characterization

Transmission electron microscopy (TEM) analysis was done in a CM120 Philips microscope, operating at 120 kV. The ultrathin sectioning was made at −80°C using a Reichert Ultracut FC4 ultracryomicrotometer, from Leica. All TEM images were analyzed without staining.

Rheological characterization

Before all rheological characterization was made, the samples were dried at 80°C for 14 h. Measurements of steady state shear viscosity $\eta(\dot{\gamma})$ at low shear rates and first normal stress difference $N_1(\dot{\gamma}) = (\tau_{11} - \tau_{22})$, where τ_{11} and τ_{22} are the tensions along the flow and perpendicular to the flow directions,[17] respectively, were made in a controlled strain rheometer, model ARES from Rheometric Scientific. The shear rates were between 0.01 and 100 s^{-1}; a 25 mm parallel-plate fixture with gap of 1 mm, temperature of 250°C, and nitrogen atmosphere was used. Delay before measurement was determined from stress overshoot experiments. The $\eta(\dot{\gamma})$ at high shear rates was also measured in an Instron capillary rheometer, model 4467, with capillary length of 2.54 cm, L/D of 33, at 250°C, between 200 and 2000 s^{-1}.

The shear storage modulus G' and the shear loss modulus G'' were measured as a function of angular frequency ω (between 0.01 and 100 rad/s) and time (at a constant ω of 1.0 rad/s) during 4000 s in the earlier described controlled strain rheometer. A strain sweep test (between 0.1 and 10.0%) was done in all samples to select the strain amplitude within the linear viscoelastic range of the material; this strain amplitude was found to be 1.0% for the **Pure** and **Extruded PA6** samples, and 0.4% for the nanocomposites samples.

Stress growth and stress relaxation experiments were also done in the same controlled strain rheometer. First a shear rate $\dot{\gamma}_0 = 1\ s^{-1}$ was applied during 180 s. The shear rate was then stopped and the relaxation stresses were measured during 120 s; after relaxation, a shear rate $\dot{\gamma}_0 = 1\ s^{-1}$ was again applied during 180 s.

Measurements of creep and constrained recoil after steady shear flow were done in a controlled stress rheometer AR-G2, from TA Instruments, using a 25 mm parallel-plate fixture with gap of 1 mm and temperature of 250°C. During the creep experiments, a shear stress of 1000 Pa was applied during 2 min. To measure the constrained recoil, this shear stress was suddenly removed. In both experiments, the shear strain was monitored as a function of time. The recovery strain γ_r after 2 min was calculated from the following relationship:

$$\gamma_r = \left[\frac{\gamma_{\text{total}} - \gamma_{\text{final}}}{\gamma_{\text{total}}}\right] \cdot 100 \quad (4)$$

in which γ_{total} is the strain after 2 min of stress application and γ_{final} is the strain after 2 min of stress removal.

Films characterization

Tensile tests of the blown films were made in a tensile testing machine, model 5569 from Instron, at room temperature, following ASTM-889 standard procedure, along the machine direction (MD) and transversal direction (TD) of the films. The elastic modulus E was determined at 25 mm/min crosshead speed, whereas all the other tensile characteristics were measured at 500 mm/min. At least five measurements of each sample were done.

Dynamic mechanical thermal analyses (DMTA) of the films were done in a controlled strain rheometer, model ARES from Rheometric Scientific, using the torsion mode at a frequency $\omega_o = 10.0$ rad/s, strain amplitude $\gamma_o = 1.0\%$, between 25 and 125°C, under nitrogen atmosphere and at a heating rate of 2°C/min. Strips of 40 mm along MD were used as samples.

The films optical properties (total haze and transmittance) were measured in a spectrophotometer from BYK Gardener, model Haze-Gard Plus, following ASTM D1003 standard procedure.

To analyze the films roughness, its surface was analyzed by atomic force microscopy (AFM) using a MMA FM-2 equipment from Veeco Digital

Instruments, with head of 1 μm, in the tapping mode. The average surface roughness of the films R_a was determined in a 10 μm × 10 μm area using the software NanoScope IIIa.

The water vapor permeability rate (WPTR) was measured following ASTM F1249-01 standard test on a Permatran equipment, model W3/31 with infrared sensor, from Mocon, at 38°C and relative humidity of 90%. The oxygen permeability rate (OTR) was measured following ASTM D3985 standard test by the coulometric method, in an Oxtran equipment, model ST, from Mocon, with pure oxygen, at 23°C and pressure of 1 atm. In both permeability tests, the net flux of permeant was perpendicular to the MD and TD of the films and parallel to the thickness direction, ND.

The thickness of the films was measured using a micrometer with planar nib, model 732, from Starrett, with resolution of 0.001 mm.

RESULTS AND DISCUSSION

Thermal characterization of the nanoclay

Figure 3 shows the results of the TGA of the C30B nanoclay.

Analyzing the derivative of the thermogravimetric (DTG) curve, three peaks at temperatures in which a maximum mass loss rate occurred were observed. The first one, at 45°C, was correlated to water loss; the second one, at 275°C, was related to mass loss of the organic components (surfactant and other chemicals); and the third one was correlated to dehydroxylation of the aluminosilicate.[16,18] Decomposition temperatures in high-resolution TGA (as defined by the DTG peaks) will be lower than the ones observed in a conventional TGA because the sample temperature is not raised until gaseous evolution at that particular temperature is completed.[18] Thus, the C30B surfactant was found to be stable up to ~ 200°C.

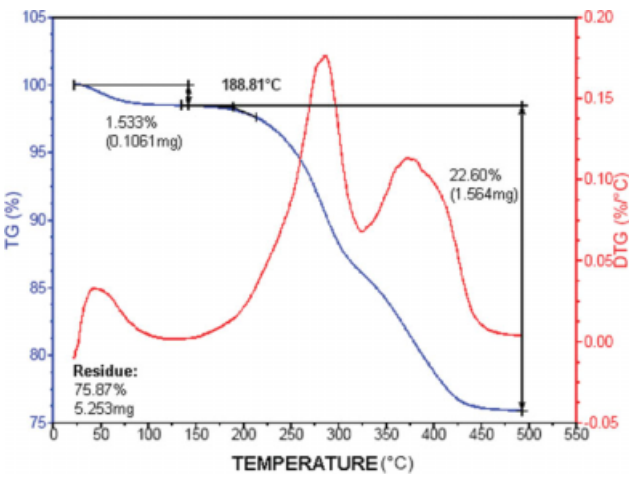

Figure 3 Thermogravimetric analysis of the C30B nanoclay. [Color figure can be viewed in the online issue, which is available at www.interscience.wiley.com.]

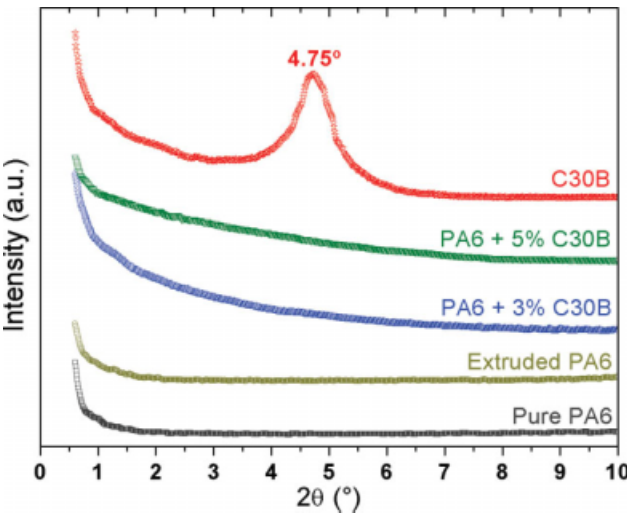

Figure 4 WAXD diffractograms of the extruded nanocomposites. [Color figure can be viewed in the online issue, which is available at www.interscience.wiley.com.]

Characterization of the extruded nanocomposites

The WAXD diffractograms of the extruded nanocomposites are shown in Figure 4.

The nanoclay's main diffraction peak occurred at $2\theta = 4.75°$ ($d_{001} = 1.87$ nm). In the nanocomposites this peak disappeared, showing that the nanoclay's lamellae were randomly distributed in the polymer; therefore, both nanocomposites had an exfoliated structure. This result was confirmed by TEM analyses; Figure 5(a) shows a TEM micrographs of the 5 wt % extruded nanocomposite. The nanoclay's lamellae are well distributed within the polyamide matrix; however, a high degree of orientation along the flow direction of the cylindrical die is observed.

Figure 6 shows the shear viscosity and the first normal stress difference of the extruded nanocomposites at 250°C.

The **Pure PA6** and the **Extruded PA6** samples had similar rheological behavior: Newtonian between 0.01 and 0.04 s^{-1}, pseudoplastic between 0.04 and 0.2 s^{-1}, Newtonian again between 0.2 and 2 s^{-1}, and pseudoplastic after 2.0 s^{-1}, probably as result of competition between chain breaking and postpolymerization reactions. The zero shear viscosity η_0 of the **Extruded PA6** sample was, however, slightly lower than that of the **Pure PA6** sample, as shown in Table I; this slight reduction could be caused by the surging of branching, degradation, and/or entanglement breakdown, among others in the **Extruded PA6** sample.

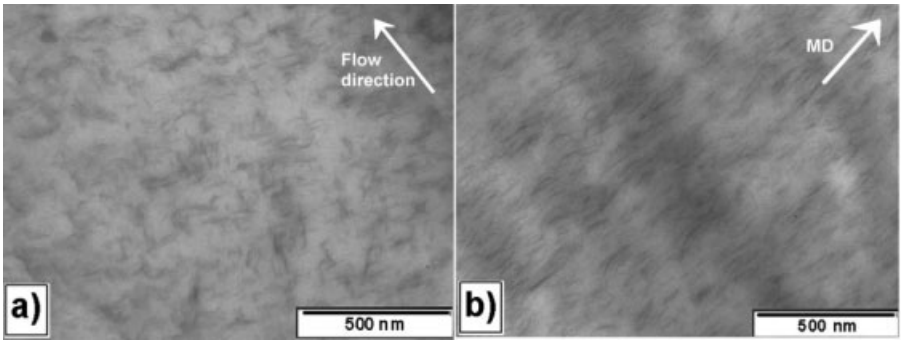

Figure 5 (a) Extruded **PA6 + 5% C30B** and (b) Blown film **PA6 + 5% C30B** (magnification ×31,000).

On the other hand, the nanocomposites were Newtonian between 0.01 and 0.03 s^{-1}, becoming pseudoplastic after this latter shear rate; that is, they attained pseudoplasticity at a lower shear rate than the **Pure PA6** sample, probably due to the alignment of the nanoclay's lamellae along the flow direction. The power law index, n, was 0.53 for the **Pure PA6**, 0.48 and 0.47 for the nanocomposites with 3 and 5 wt %, respectively, as shown also in Table I; that is, the nanocomposites were more pseudoplastic than the **Pure PA6**. Another significant difference was observed: the zero shear viscosity η_0 of the nanocomposites was significantly higher than of the **Pure PA6** (Table I). This increase in η_0 can be attributed to the formation of a percolated network as result of the physical and chemical interactions (pseudoentanglements) between the macromolecular chains and the nanoclay's lamellae.[12,19,20] The percolated network will have, therefore, a higher flow resistance than the pure polymer.

$N_1(\dot{\gamma})$ was negative in the measured shear rate range, that is, the materials had high elasticity during shear, being the nanocomposites more elastic than the pure polymers.

Figure 7 shows the dynamic rheological properties of the extruded nanocomposites at 250°C.

Both modules increased proportionally to the increase in amount of nanoclay, as other works have confirmed.[21] The **Pure PA6** displayed three of the standard viscoelastic regions of a $G'(\omega)$ curve: the terminal, the plateau and the transition zones. The modulus at the plateau, G_N^0, is inversely proportional to the molecular weight between entanglements, M_e.[22] In the **Extruded PA6** and nanocomposites samples, this plateau almost disappeared, but if a horizontal line is traced at the end of the transition zone,[22] it is observed that as the amount of nanoclay increased, G_N^0 increased (Table I) and thus, M_e decreased. That is, the nanoclay's lamellae acted as entanglement points in the nanocomposites decreasing M_e. The **Extruded PA6** sample had, on the other hand, a lower G_N^0 than the **Pure PA6**; that is, M_e (**Extruded PA6**) > M_e (**Pure PA6**). Linear polymers have a higher amount of entanglements (lower M_e) than branched ones; thus, probably the postpolymerization of the residual monomer in the PA6 produced more branched chains than linear ones.

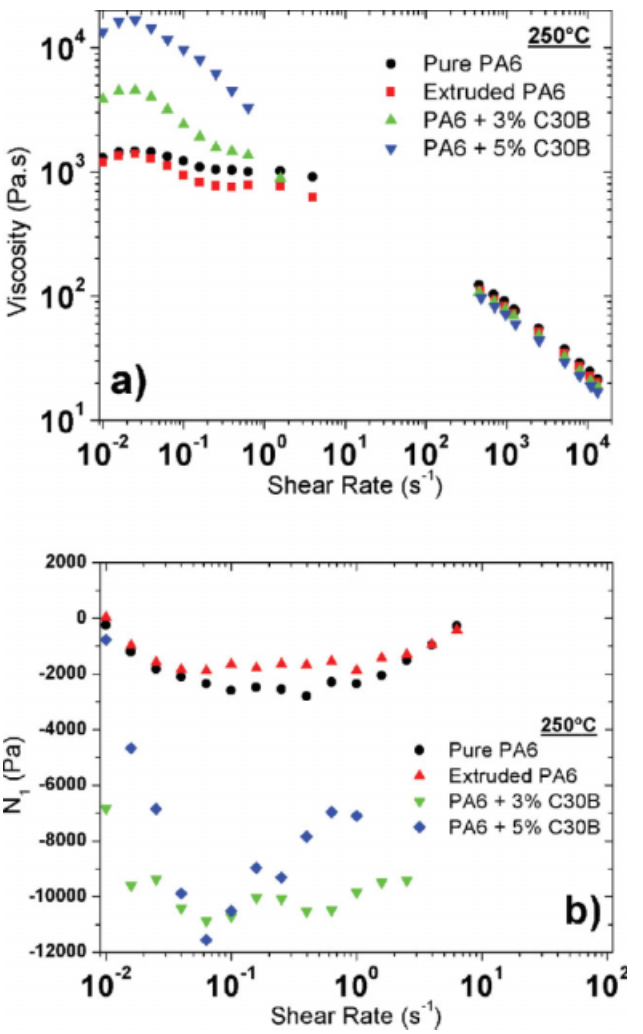

Figure 6 Extruded PA6/MMT nanocomposites: (a) Shear viscosity and (b) First normal stress difference, both at 250°C. [Color figure can be viewed in the online issue, which is available at www.interscience.wiley.com.]

TABLE I
Rheological Parameters of the Samples, at 250°C

Materials	Power law index, n	Zero shear viscosity, η_0 (Pa s)	Modulus at the plateau G_N^o (Pa)	Frequency of the crossing point, ω_c (rad/s)	Relaxation time, t_r (s)	Slope G' (ω)	Slope G'' (ω)
Pure PA6	0.53	1474	~1975	1.58	0.63	1.89	1.02
Extruded PA6	0.56	1345	~839	0.63	1.58	1.96	0.96
PA6 + 3% C30B	0.48	4538	~20965	25.12	0.04	0.86	0.31
PA6 + 5% C30B	0.47	16302	~47863	–	→0	0.75	0.02

The crossover frequency, ω_c (where $G' = G''$), also changed with the increase in nanoclay loading and molecular weight (MW), as observed in Table I. A polymer relaxation time, t_r, can be defined as follows:

$$t_r = 1/\omega_c \quad (5)$$

The relaxation times of the samples are also shown in Table I. The **Extruded PA6** had lower ω_c (and higher t_r) than the **Pure PA6**; that is, the MW (**Extruded PA6**) > MW (**Pure PA6**), due to postpolymerization of the residual monomer. On the other hand, as the amount of nanoclay increased, ω_c increased and t_r decreased. This result, as pointed out also by Smakande et al.,[23] was surprising, because it would expect that the nanoclay's lamellae would retard the relaxation of the polymer chains. Thus, the dominant relaxation mode in the nanocomposites was of the PA6 chains, and if t_r decreased, this is an evidence that the MW of the PA6 in the nanocomposites also decreased. This decrease could have been caused by two different factors: (i) the residual monomer interacted first and preferentially with the nanoclay surfactant; thus, no further postpolymerization occurred in the nanocomposite, as it had occurred in the **Pure PA6** and **Extruded PA6** samples; (ii) the presence of the nanoclay helped to increase the thermal degradation of the PA6 in the nanocomposite and chains breaking reactions were dominant. However, if the last behavior were predominant, the shear viscosity of the nanocomposite would be lower than that of the Pure PA6 and Extruded PA6 samples, which did not occur. Therefore, we concluded that in the nanocomposite, part of the residual monomer interacted first with the nanoclay's surfactant, avoiding the complete formation of branching.

Regarding the slope of the terminal zone, the **Pure PA6** and the **Extruded PA6** had the standard slopes of a polymer melt ($G' \sim \omega^2$ and $G'' \sim \omega^1$); however, with the addition of the nanoclay, the $G'(\omega)$ slope changed to lower values ($G' \sim \omega^1$), whereas the $G''(\omega)$ slope changed to values near 0 ($G'' \sim \omega^0$), as shown in Table I. Both slopes tending to 0 ($G' \sim \omega^0$, $G'' \sim \omega^0$) would represent the behavior of a pseudo-solid material, with a percolated network and a well disperse structure[3,24–26]; thus, both PA6 nanocomposites were percolated and well disperse, as already confirmed by the TEM micrographs.

The time stability of the nanocomposites structures was analyzed by measuring G' and G'' as a

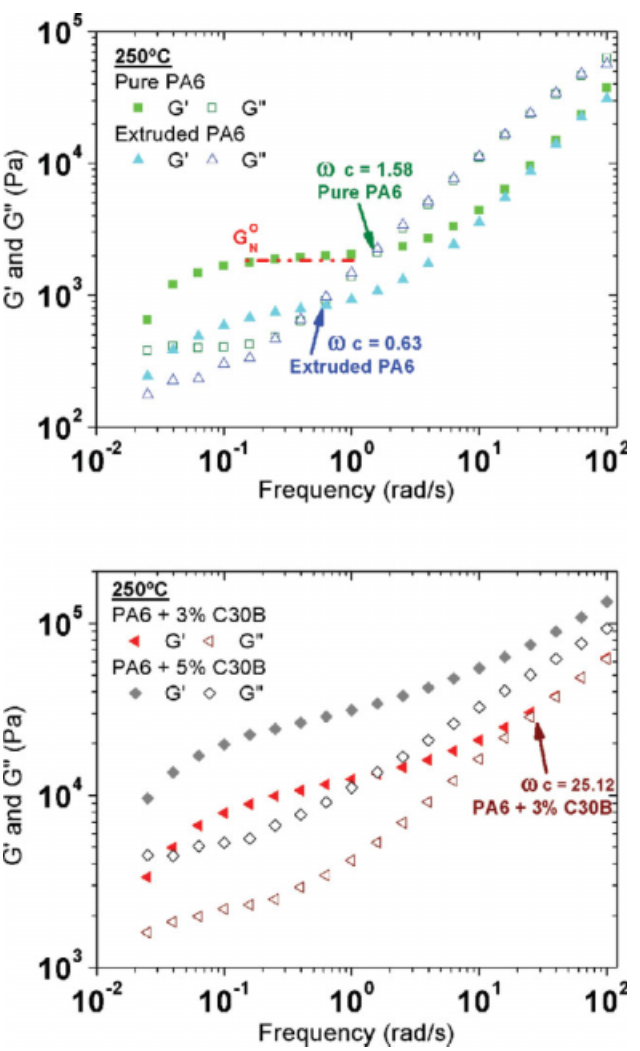

Figure 7 Dynamic rheological properties of the extruded nanocomposites, at 250°C. [Color figure can be viewed in the online issue, which is available at www.interscience.wiley.com.]

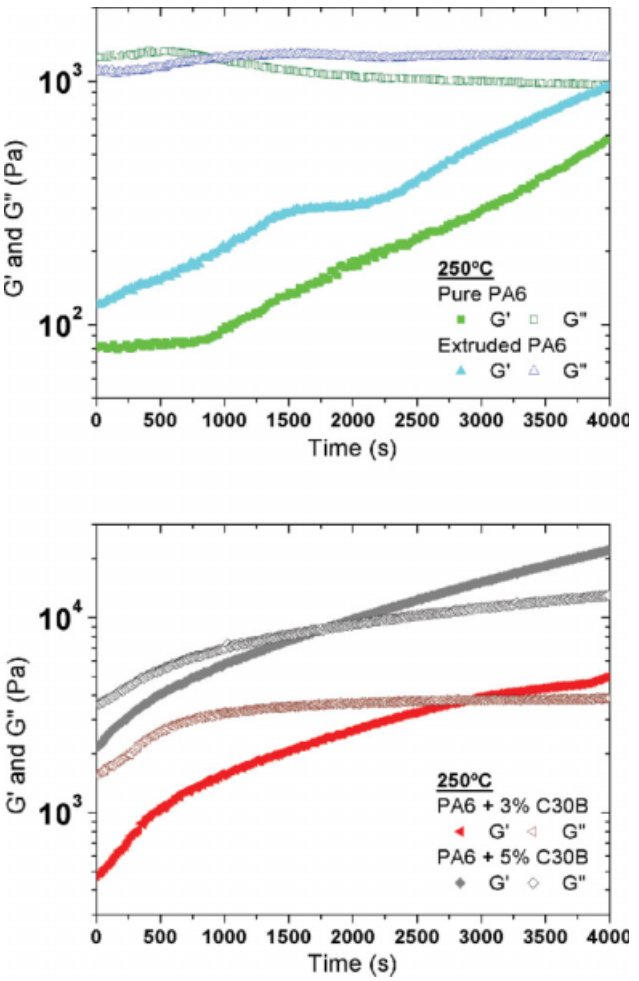

Figure 8 Storage and loss modules of the nanocomposites as a function of time (250°C). [Color figure can be viewed in the online issue, which is available at www.interscience.wiley.com.]

function of time, at 250°C. Figure 8 shows these measurements.

The storage modulus of all the samples increased with time, showing that the residual monomer was still present, even after the twin-screw extrusion. The increase in elasticity was stronger than the increase in viscosity confirming again that the residual monomer postpolymerization produced more branched chains than linear ones.

The results of the stress growth and stress relaxation experiments, at 250°C, are shown in Figure 9.

The stress overshooting of both PA6 samples was similar (around 1200 Pa); in the nanocomposites, on the other hand, the higher the amount of nanoclay, the higher the stress overshooting, being 2500 and 3400 Pa for the 3 wt % and 5 wt % nanocomposites, respectively. The high stress overshooting is again an indication of strong interactions between the polymer chains and the nanoparticles. The stress relaxation of the **Pure PA6** was quicker than of the **Extruded PA6** samples, that is, the higher the MW

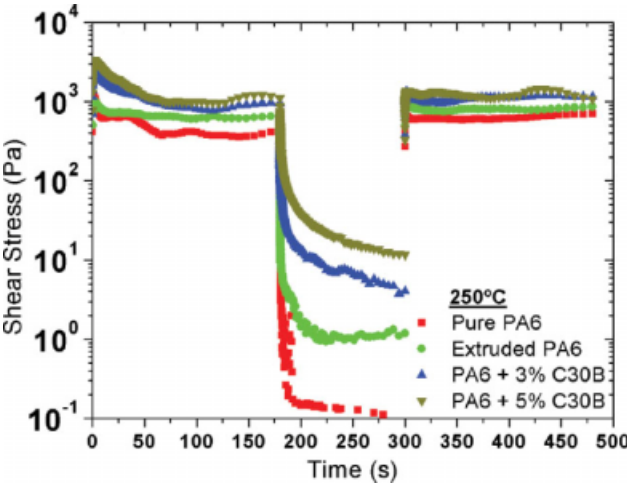

Figure 9 Stress growth and stress relaxation experiments of the extruded nanocomposites, at 250°C and $\dot{\gamma}_0 = 1.0$ s^{-1}. [Color figure can be viewed in the online issue, which is available at www.interscience.wiley.com.]

the slower the stress relaxation. Also in the nanocomposites, the higher the amount of nanoclay, the slower the stress relaxation.

The constrained recoil of the extruded nanocomposites after cessation of the steady state shear flow, at 250°C, is shown in Figure 10.

During the creep experiment, the **Pure PA6**, **Extruded PA6**, and the 3 wt % nanocomposite deformed similarly; the **Extruded PA6** sample, however, had the highest total deformation of all the samples, as shown in Table II (confirming the plasticization effect promoted by the branched chains). On the other hand, the 5 wt % nanocomposite had the lowest total deformation. This latter result can be an indication of strong polymer-particle interactions; that is, the macromolecules, being linked to the solid

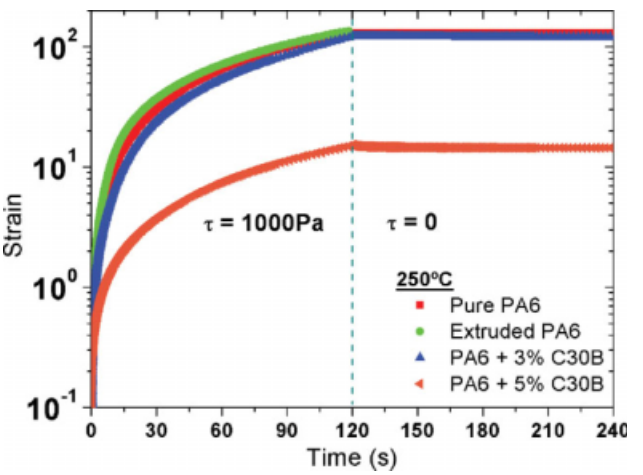

Figure 10 Constrained recoil after cessation of steady state shear flow ($\tau = 1000$ Pa), at 250°C. [Color figure can be viewed in the online issue, which is available at www.interscience.wiley.com.]

TABLE II
Strain Recoil of the Extruded Nanocomposites, at 250°C after 2 min

Materials	γ_{total}	γ_{final}	γ_r (%)
Pure PA6	131.24	130.93	0.24
Extruded PA6	136.16	135.00	0.85
PA6 + 3% C30B	121.97	121.37	0.49
PA6 + 5% C30B	14.97	14.61	2.40

nanoparticles will have their motions restricted and thus, will be less deformed. All the samples had, however, very small recoil, as also shown in Table II; again, the 5 wt % nanocomposite was the more elastic of the extruded materials.

Blown films production and characterization

Table III shows the pressure developed at the extruder die during the film blowing process. The formation of branches in the **Pure PA6** and the alignment of the nanoclay lamellae along the flow made the die pressure strongly decrease.

The bubble stability during the blowing of the nanocomposites films was slightly higher than of the **Pure** and **Extruded PA6**, as expected from the dynamic rheological result (the higher the G', the higher the bubble stability); thus, blown films of all the materials were successfully obtained.

The stress versus strain curves of the blown films along MD and TD are shown in Figure 11 whereas in Tables IV and V the values of elastic modulus E, yield stress σ_y, ultimate stress σ_r, ultimate strain ε_r, and toughness are tabulated. Along MD, the best mechanical properties were obtained with the 5 wt % nanocomposite, whereas along TD the 3 wt % nanocomposite had the best.

Along MD, the elastic modulus of the blown films of the 3 and 5 wt % nanocomposites were 27 and 47%, respectively, higher than of the blown film of the **Pure PA6**, whereas along TD, these modules were both 80% higher than of the **Pure PA6**. The yield stress along MD also increased in the nanocomposites' blown films: the 3 and 5 wt % nanocomposites both had an increase of 21% over the **Pure PA6** blown film. All the other properties of the films, however, had a slight decrease compared with the **Pure PA6** blown film.

TABLE III
Pressure Developed at the Extruder Die During the Film Blowing Process

Films	Pressure (Kgf/cm^2)
Pure PA6	300
Extruded PA6	290
PA6 + 3% C30B	134
PA6 + 5% C30B	128

Figure 12 shows the DMTA curves of the blown films; the glass transition temperature T_g (maximum of tan δ) was calculated from these curves. The 5 wt % nanocomposite had the highest T_g (79.6°C) of all the films, an increase of ~ 8°C over the T_g of the **Pure PA6** blown film (71.3°C). The 3 wt % nanocomposite also had an increase in T_g (75.7°C) over the T_g of the **Pure PA6** blown film. These results confirm the anchoring of the macromolecules chains by the nanoclay's lamellae, which will restrict the chains motion, increasing the T_g. The amount of amorphous phase (proportional to the height of the tan δ peak) was the highest in the **Pure PA6** blown film and the 3 wt % nanocomposite and was responsible for their high ultimate tensile mechanical properties. On the other hand, the lower amount of amorphous phase present in the 5 wt % nanocomposite was responsible for its high elastic modulus.

The optical properties of the films are shown in Table VI. The nanoclay influenced mostly the haze of the films decreasing this property; however, the level of transmittance of the samples was not

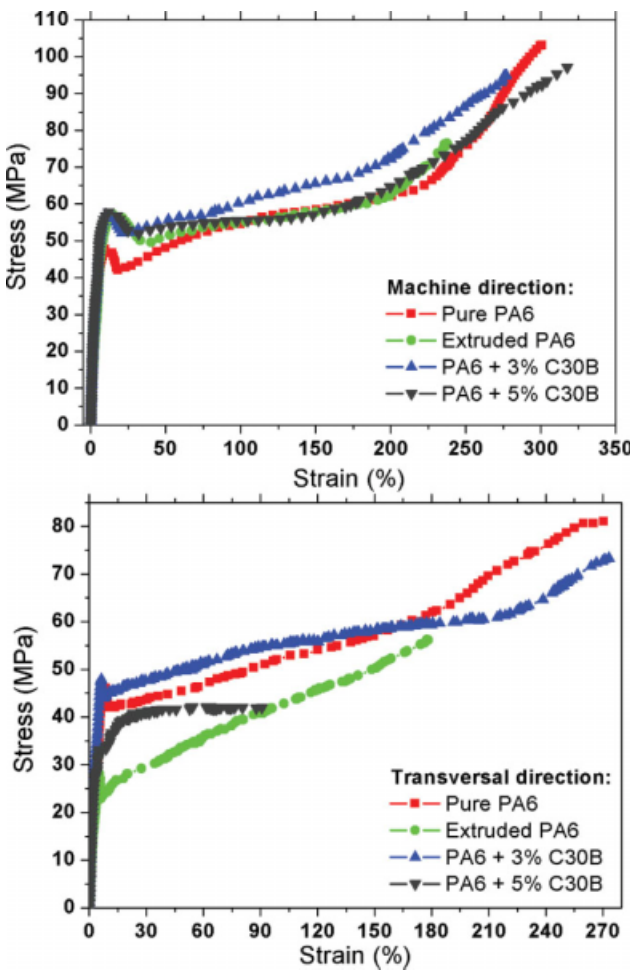

Figure 11 Tensile curves of the blown films along MD and TD. [Color figure can be viewed in the online issue, which is available at www.interscience.wiley.com.]

TABLE IV
Tensile Mechanical Properties of the Blown Films Along MD

Films	E (MPa)	σ_y (MPa)	σ_r (MPa)	ε_r (%)	Toughness (10^{12} J/m^3)
Pure PA6	1159.4 ± 94.9	47.1 ± 1.8	101.8 ± 2.9	297.7 ± 42.2	1.841
Extruded PA6	758.3 ± 37.5	57.1 ± 0.8	74.7 ± 1.0	236.5 ± 46.0	1.359
PA6 + 3% C30B	1471.7 ± 95.8	57.2 ± 1.1	97.1 ± 0.7	276.7 ± 57.8	1.847
PA6 + 5% C30B	1700.0 ± 131.4	57.7 ± 0.9	92.6 ± 0.6	317.8 ± 27.5	2.042

TABLE V
Tensile Mechanical Properties of the Blown Films Along TD

Films	E (MPa)	σ_y (MPa)	σ_r (MPa)	ε_r (%)	Toughness (10^{12} J/m^3)
Pure PA6	602.7 ± 50.9	46.1 ± 2.0	80.1 ± 0.7	270.5 ± 90.1	1.552
Extruded PA6	639.1 ± 112.1	27.5 ± 0.7	57.2 ± 1.1	176.8 ± 51.3	0.717
PA6 + 3% C30B	1083.2 ± 81.7	47.7 ± 1.2	74.9 ± 1.2	272.5 ± 37.4	1.538
PA6 + 5% C30B	1081.6 ± 43.9	39.2 ± 1.2	41.6 ± 3.7	89.4 ± 22.1	0.583

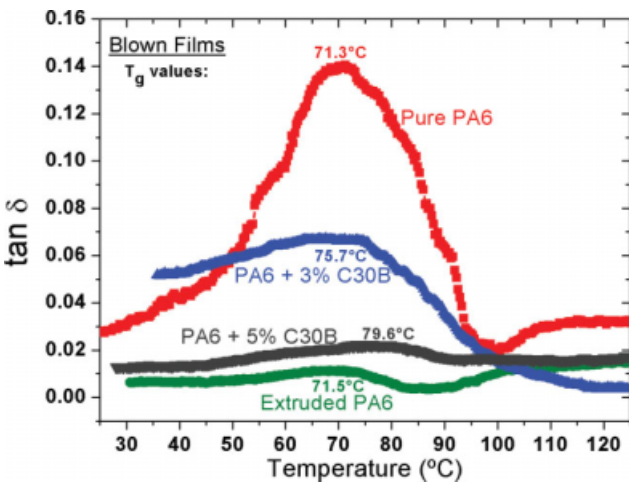

Figure 12 DMTA analyses of the blown films. [Color figure can be viewed in the online issue, which is available at www.interscience.wiley.com.]

affected by the nanoclay. The brightness was not measured, but it was observed that the nanocomposites films were brighter than the **Pure PA6** film.

Figure 13 shows the AFM micrographs of the surface of the blown films. The surface roughness R_a was calculated from the micrographs as described in our previous work.[3]

Similar to results of our earlier studies of blown films of HDPE/MMT,[3] the roughness of the blown films of the PA6 nanocomposites was slightly reduced by the nanoclay's presence, as shown in Table VI.

The nanoclay distribution in the PA6 matrix was also analyzed by TEM; micrographs of the 5 wt % blown films are shown in Figure 5(b). A high orientation of the nanoclay's lamellae along MD is observed.

The WPTR and OTR of the blown films are shown in Table VII. Both permeation rates decreased compared to the permeation rate of the **Pure PA6** blown film. The WPTR of the blown films of the 3 and 5 wt % nanocomposites decreased 20 and 34%, respectively, compared to the **Pure PA6** blown film. The OTR of the blown films of the 3 and 5 wt % nanocomposites decreased 8 and 31%, respectively, compared to the **Pure PA6** blown film. That is, the use of the nanoclay improved the water vapor and oxygen permeabilities of the blown films, due to a tortuosity effect; because the nanoclay's lamellas were aligned parallel to MD and therefore, perpendicular to the penetrant net flux, the penetrant molecules had to diffuse thru a lengthier path.

TABLE VI
Transmittance, Haze, and Roughness of the Blown Films

Films	Transmittance (%)	Haze (%)	R_a (nm)
Pure PA6	92.1 ± 0.3	21.6 ± 2.0	26 ± 4
Extruded PA6	91.4 ± 0.1	27.5 ± 3.7	27 ± 8
PA6 + 3% C30B	91.6 ± 0.3	11.0 ± 2.3	20 ± 3
PA6 + 5% C30B	91.3 ± 0.2	11.6 ± 2.5	22 ± 2

CONCLUSIONS

Exfoliated nanocomposites (3 and 5 wt %) of PA6 (with residual monomer) and an organically treated montmorillonite were successfully produced by twin-screw extrusion. The rheological characterization of the extruded nanocomposites allowed concluding that the postpolymerization of the residual monomer in the PA6 produced more branched chains than linear ones, that the nanoclay's lamellas acted as entanglement points in the nanocomposites and that the MW of the PA6 in the nanocomposites decreased. In the nanocomposite, part of the residual

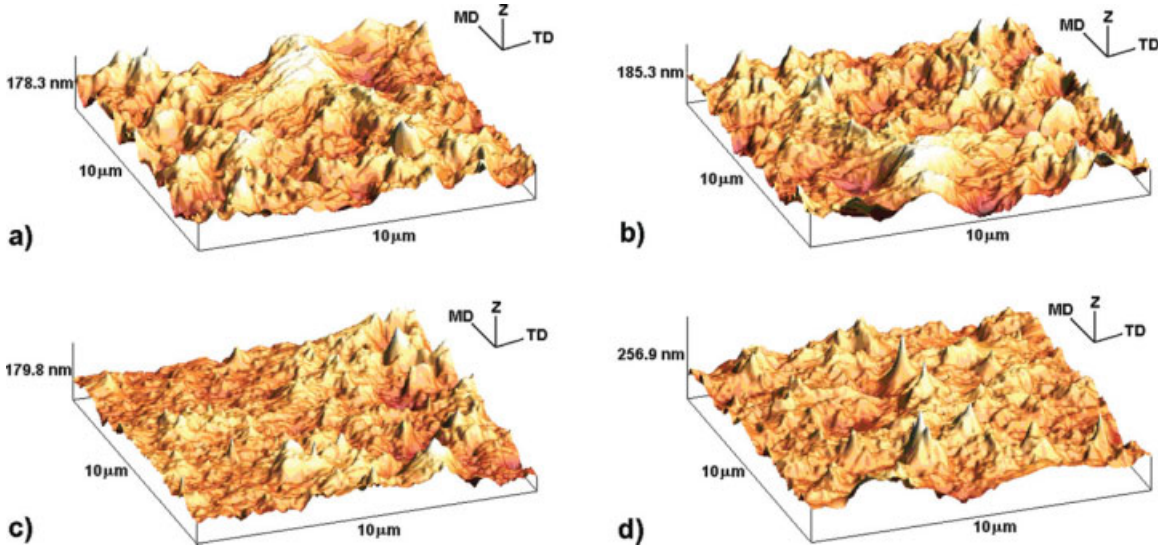

Figure 13 AFM micrographs of the surface of the blown films of: (a) **Pure PA6**, (b) **Extruded PA6**, (c) **PA6 + 3% C30B**, and (d) **PA6 + 5% C30B**. [Color figure can be viewed in the online issue, which is available at www.interscience.wiley.com.]

monomer interacted first with the nanoclay's surfactant, avoiding the complete formation of branching.

The high stress overshooting was an indication of strong interactions between the polymer chains and the nanoparticles. The 5 wt % nanocomposite had the lowest total deformation and was the more elastic of the extruded materials.

Blown films of the nanocomposites were also successfully produced; due to the alignment of the nanoclay lamellas along the flow, the die pressure during the film blowing process strongly decreased. Along MD, the best mechanical properties were obtained in the 5 wt % nanocomposite, while along TD the 3 wt % nanocomposite was the best. The 5 wt % nanocomposite also had the highest T_g of all the films.

The nanoclay influenced mainly the haze of the films, decreasing this property; however, the level of transmittance of the samples was not affected by the nanoclay. The brightness of the nanocomposites films was observed to be higher than of the **Pure PA6** film.

TABLE VII
Water Vapor and Oxygen Permeation Rates of the Blown Films

Films	WPTR [g(water)/ m^2 day]/μm[a]	OTR [mL(NCTP)/ m^2 day]/μm[a]
Pure PA6	1.32 ± 0.17	0.13 ± 0.01
Extruded PA6	1.35 ± 0.16	0.12 ± 0.01
PA6 + 3% C30B	1.05 ± 0.14	0.12 ± 0.01
PA6 + 5% C30B	0.87 ± 0.11	0.09 ± 0.02

[a] Normalized by the films thickness.

The use of the nanoclay improved the water vapor and oxygen permeability of the nanocomposites blown films due to a tortuosity effect; because the nanoclay's lamellas were aligned along MD, the molecules of the penetrant (water vapor or oxygen) had to diffuse thru a lengthier path.

The authors thank Rhodia Engineering Plastics from Brazil for the PA6 donation, Max-Planck Institute for Polymer Research, Deutscher Akademischer Auslandsdienst for the cryoultramicrotome donation, and J. Marini and M. M. Favaro for the help in the dynamic rheological measurements.

References

1. Brosy, A. L.; Marsh, K. S. Encyclopedia of Packaging Technology; Wiley: New York, 1997.
2. Alexandre, M.; Dubois, P. Mater Sci Eng 2000, 28, 1.
3. Lotti, C.; Isaac, C. S.; Branciforti, M. C.; Alves, R. A.; Liberman, S.; Bretas, R. E. S. Eur Polym J 2008, 44, 1346.
4. Fornes, T. D.; Paul, D. R. Polymer 2003, 44, 4993.
5. Zhao, J.; Morgan, A. B.; Harris, J. D. Polymer 2005, 46, 8641.
6. Shah, R. K.; Krishnaswamy, R. K.; Takahashi, S.; Paul, D. R. Polymer 2006, 47, 6187.
7. Gu, S. Y.; Ren, J.; Wang, Q. F. J Appl Polym Sci 2003, 91, 2427.
8. Baldi, F.; Franceschini, A.; Bignotti, F.; Tieghi, G.; Riccò, T. Rheol Acta 2009, 48, 73.
9. Tung, J.; Gupta, R. K.; Simon, G. P.; Edward, G. H.; Bhattacharya, S. N. Polymer 2005, 46, 10405.
10. Picard, E.; Vermogen, A.; Gérard, J.-F.; Espuche, E. J Membr Sci 2007, 292, 133.
11. Picard, E.; Gérard, J.-F.; Espuche, E. J Membr Sci 2008, 313, 284.
12. Alexandre, B.; Langevin, D.; Médéric, P.; Aubry, T.; Couderc, H.; Nguyen, Q. T.; Saiter, A.; Marais, S. J Membr Sci 2009, 328, 186.
13. Beatrice, C. A. G. Master Thesis, Universidade Federal de São Carlos, 2008.

14. Rhodia Engineering Plastics. Available at: http://www.rhodia-ep.com; accessed on 3 December 2008.
15. Mazzafero. Available at: http://www.mazzaferro.com.br; accessed on 16 February 2009.
16. Southern Clay Products Inc. Available at: http://www.nanoclay.com; accessed on 3 December 2008.
17. Bretas, R. E. S.; D'Avila, M. A. Reologia de polímeros fundidos; EdUFSCar: São Carlos, 2005.
18. Xie, W.; Gao, Z.; Pan, W.; Hunter, D.; Singh, A.; Vaia, R. Chem Mater 2001, 13, 2979.
19. Shen, L.; Lin, Y.; Du, Q.; Zhong, W.; Yang, Y. Polymer 2005, 46, 5758.
20. Favaro, M. M.; Branciforti, M. C.; Bretas, R. E. S. In Proceedings of the 9th Brazilian Polymer Congress (CBPol); Brazilian Polymer Association: Campina Grande, Brazil, 2007.
21. Aubry, T.; Razafinimaro, T.; Médéric, P. J Rheol 2005, 49, 425.
22. Ferry, J. D. Viscoelastic Properties of Polymers; Willey: New York, 1980.
23. Samakande, A.; Sanderson, R. D.; Hartmann, P. C. Polymer 2009, 50, 42.
24. Wagener, R.; Reisinger, T. J. G. Polymer 2003, 44, 7513.
25. Durmus, A.; Kasgoz, A.; Macosko, C. W. Polymer 2007, 48, 4492.
26. Tjong, S. C. Mater Sci Eng 2006, 53, 73.